Instant Dehazing of Images Using Polarization

Yoav Y. Schechner, Srinivasa G. Narasimhan and Shree K. Nayar
Department of Computer Science, Columbia University, New York, NY 10027
{yoav,srinivas,nayar}@cs.columbia.edu

Abstract

We present an approach to easily remove the effects of haze from images. It is based on the fact that usually airlight scattered by atmospheric particles is partially polarized. Polarization filtering alone cannot remove the haze effects, except in restricted situations. Our method, however, works under a wide range of atmospheric and viewing conditions. We analyze the image formation process, taking into account polarization effects of atmospheric scattering. We then invert the process to enable the removal of haze from images. The method can be used with as few as two images taken through a polarizer at different orientations. This method works instantly, without relying on changes of weather conditions. We present experimental results of complete dehazing in far from ideal conditions for polarization filtering. We obtain a great improvement of scene contrast and correction of color. As a by product, the method also yields a range (depth) map of the scene, and information about properties of the atmospheric particles.

1 Introduction

Recently there has been a growing interest in the analysis of images of scenes affected by weather phenomena. The main objective has been to enhance [6, 10, 15, 24] images taken in poor visibility, and even restore the clear-day visibility of the scene [11, 12, 14]. It has also been observed that degradation of images by atmospheric scattering can actually be exploited to obtain information about the scene, particularly its range map [4, 12, 14]. Some image enhancement methods proposed in the past require prior information about the scene (e.g., distances [15, 24]). Other methods are based on specialized radiation sources and detection hardware [16, 23].

Computer vision methods have restored clear-day visibility of scenes using neither special radiation sources nor external knowledge about the scene structure or aerosols [11, 14]. These methods rely only on the acquired images, but require weather conditions to change between image acquisitions. This can take too long to make dehazing practical. They also require that the scattering properties will not vary with wavelength. This paper describes an approach that does not need the weather conditions to change, and can thus be applied instantly. Moreover, in this approach the scattering properties may vary with wavelength.

Our approach is based on analyzing images taken through a polarizer. Polarization filtering has long been used in photography through haze [20]. Relying only on optical filtering is, however, restrictive: it is sufficient only on clear days, with weak light scattering (mainly due to air molecules), when the sun is $\approx 90^o$ to the viewing direction [9, 20]. In these situations photographers set the polarization filter at an orientation that best improves image contrast. In general, however, polarization filtering alone *cannot* remove the haze from images. Here, we obtain much more than optics alone can yield by analyzing the polarization filtered images.

The analysis of polarization filtered images has proved to be useful for computer vision. For example, it was used to analyze specularities [13, 17, 25], separate transparent and semi-reflected scenes [7, 18, 19], classify materials [26], and segmenting scenes [1]. We note that advances in polarimetric cameras [1, 21, 25, 26] enable acquisition of polarization information in real time.

In this paper we model the image formation process, taking into account polarization effects of atmospheric scattering in haze. We then use this model to recover the dehazed scene, and also obtain information about scene structure and atmospheric properties. Our approach *does not* require modeling of the scattering particles' size or their precise scattering mechanisms. The principle is very simple: the image is composed of two unknown components - the scene radiance in the absence of haze, and airlight (the ambient light scattered towards the viewer). To recover these two unknowns we need two independent images. We easily obtain these images because usually airlight is partially polarized. The method only requires that the airlight induces *some* detectable partial polarization. We demonstrate removal of haze effects from a real scene in a situation where pure optical filtering (without applying our algorithm) does *not* suffice at all.

2 Theoretical Background

2.1 Airlight Polarization

One of the causes for image degradation associated with atmospheric scattering is *airlight*. In this process, light coming from the illumination sources (e.g., the sun) is scattered towards the viewer [14]. Consider Fig. 1. The airlight

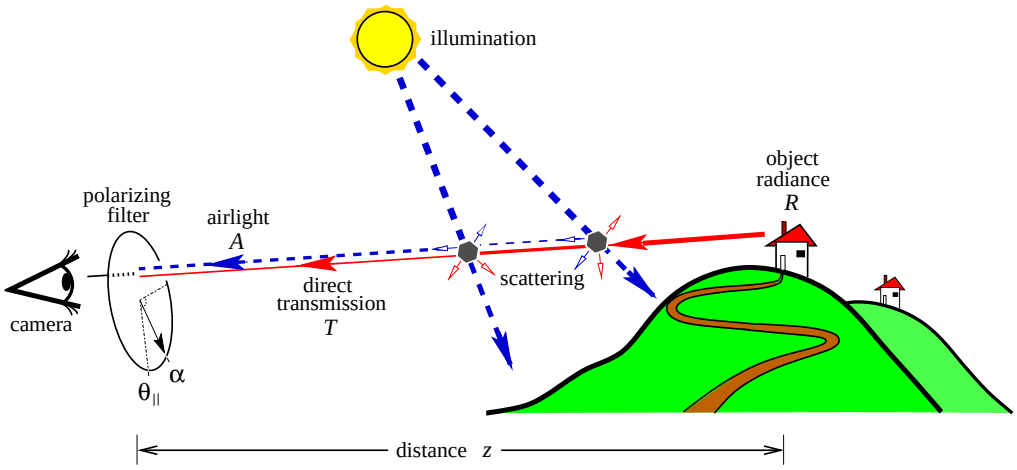

Figure 1. [Dashed rays] Light coming from the illuminant (e.g., sun) and scattered by atmospheric particles towards the camera is the airlight A. The airlight increases with the distance z of the object. [Solid ray] The light emanating from the object R is attenuated by scattering along the line of sight, leading to the direct transmission T. The direct transmission decreases with z. The scene is imaged through a polarizing filter at angle α. The polarization component parallel to the plane of incidence is best transmitted through the filter at $\alpha = \theta_{\|}$.

increases with the distance z from the object:

$$A = A_\infty \left(1 - e^{-\beta z}\right) \quad , \tag{1}$$

where β is the scattering coefficient [11]. Here A_∞ is the airlight corresponding to an object at an infinite distance, which we may take as the horizon.

Assume for a moment that the illumination of any scattering particle comes from one direction (one illumination source). The light ray from the source to a scatterer and the line of sight from the camera to the scatterer define a *plane of incidence*. We divide the airlight intensity into two components[1], that are *parallel* and *perpendicular* to this plane, $A^{\|}$ and $A^{\perp}$, respectively. The scattered light is partially linearly polarized perpendicular to this plane [8, 9]. The airlight degree of polarization is

$$P \equiv \frac{A^{\perp} - A^{\|}}{A} \, , \tag{2}$$

where

$$A = A^{\perp} + A^{\|} \tag{3}$$

is the total airlight intensity given in Eq. (1). The degree of polarization greatly varies as a function of the size of the scattering particles, their density and the viewing direction. We now explain the effectiveness of polarization in various haze and illumination conditions.

2.1.1 The Trivial Case

The strongest polarization effect is observed when the scattering is caused by independent air molecules and very small dust particles (Rayleigh scattering) [3, 9, 20, 26]. Only when the light source is normal to the viewing direction, the airlight is totally polarized ($P = 1$) *perpendicular* to the plane of incidence. Thus, it can be eliminated if the image is captured through a polarizing filter oriented *parallel* to this plane. Dehazing in this case is thus trivial, because it is achieved by optical filtering alone. Note that this situation is very restricted. In contrast, our method is applicable to more general situations.

2.1.2 The General Case

In general, the airlight will not be completely polarized. Thus, the polarizing filter, on its own, cannot remove the airlight. For example, in Rayleigh scattering P decreases as the direction of illumination deviates from 90^o (relative to the viewing direction). The degree of polarization P is also decreased by *depolarization*. This is caused by multiple scatterings: an illuminant of a scattering particle may be another particle. Thus, light may undergo multiple scatterings in the atmosphere, in random directions, before hitting the particle that ultimately scatters part of this light towards the viewer. Each direction of scattering creates a different plane of incidence. Because the camera senses the sum of these scatterings, the overall degree of polarization is reduced [2]. Multiple scatterings [3, 8, 9, 20], are more probable when the particle size is large or when the density of scatterers is high (poorer visibility). To make matters more complicated, the depolarization depends on the wavelength [9, 20].

Fortunately, our algorithm *does not* require explicit modeling of the precise mechanisms of scattering. The method is based on the fact that even a partial polarization of the airlight can be exploited in post-processing to remove scattering effects. However, this degree of polarization needs to be significant enough to be detected. There are some

[1] In terms of the electric field vector associated with the airlight radiation: these are the expectation values of the squared projections of this vector, parallel and perpendicular to the plane of incidence.

weather conditions under which the algorithm will not be effective, as discussed in Sec. 8.

2.2 Direct Transmission Polarization

In addition to the presence of airlight, scattering degrades images by attenuating the light emanating from scene objects. Let the scene radiance be R in the absence of haze (scattering) between the scene and the viewer. When haze is present, as a ray of light progresses towards the viewer (Fig. 1), part of its energy is scattered to other directions. Thus, the light energy that reaches the viewer is an attenuated fraction of R, called the *direct transmission* [14]. As a function of the distance z and scattering coefficient β, the direct transmission is

$$T = Re^{-\beta z} \quad . \tag{4}$$

The scattering of the directly transmitted light does not change the polarization state [3, 8] of the incident light[2], although the overall intensity is attenuated. Therefore, the degree of polarization and the polarization direction of the transmitted light do not change along the line of sight.

The assumption we make in this paper is that light emanating from scene objects has insignificant polarization. It follows that the polarization of the direct transmission is also insignificant. This assumption is invalid for specular surfaces. Nevertheless, the polarization associated with specular objects becomes negligible when they are far enough. The reason is that the direct transmission decreases (Eq. 4) while airlight increases (Eq. 1) with distance. Thus, the polarization of the airlight dominates the measured light. Hence, the model becomes more accurate where it is needed most - for distant objects that are most affected by haze.

Note that airlight is just the aggregation of light scattered by particles at various distances along the line of sight. Since the degree of polarization of this light does not change along the line of sight, P (Eq. 2) does not depend on the distance.

3 Image formation

The overall intensity we measure is the sum of the airlight and the direct transmission. Without mounting a polarizer on the camera, the intensity is

$$I^{\text{total}} = T + A \quad . \tag{5}$$

When a polarizer is mounted, the intensity changes as a function of the polarizer orientation angle α. Fig. 2 describes the intensity at a single pixel. The intensity is a cosine function of α (See details in Appendix A.2). On average, the measured intensity is $I^{\text{total}}/2$.

One of our goals is to decouple the airlight from the direct transmission. Since we assume that direct transmission is not polarized, its energy is evenly distributed between the polarization components. The variations due to the polarizer rotation are assumed to be mainly due to the airlight. As seen in Fig. 2, when the polarizing filter is oriented parallel to the plane of incidence ($\alpha = \theta_{\parallel}$), we measure

$$I^{\parallel} = T/2 + A^{\parallel} \quad , \tag{6}$$

where (from Eqs. 2,3)

$$A^{\parallel} = A(1-P)/2 \quad . \tag{7}$$

This is the "best state" of the polarizer, because here the measured intensity is the closest to the direct transmission (except for a factor of 1/2). Still, there is a difference between $I^{\parallel}$ and $T/2$, because the airlight is not completely polarized ($A^{\parallel} \neq 0$).

In the next section, we recover T by comparing two images taken with different orientations of the polarizer. For instance, one image can be $I^{\parallel}$, while the other,

$$I^{\perp} = T/2 + A^{\perp} \tag{8}$$

is acquired when the filter is oriented perpendicular to $\theta_{\parallel}$. From Eqs. (2,3)

$$A^{\perp} = A(1+P)/2 \quad . \tag{9}$$

From Eqs. (3,6,8),

$$I^{\text{total}} = I^{\parallel} + I^{\perp} \quad . \tag{10}$$

Note that $I^{\perp}$ is the "worst state" of the polarizer, because the airlight is enhanced relative to the direct transmission. In order to dehaze the image we first have to remove the airlight. The key for that is the estimation of P. As shown

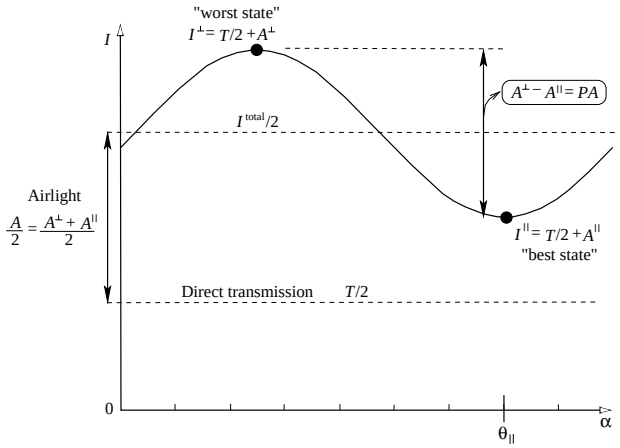

Figure 2. At each pixel, the minimum measured intensity as a function of α is $I^{\parallel}$. The maximum is $I^{\perp}$. The difference between these measurements is due to the difference between the airlight components $A^{\parallel}, A^{\perp}$. It is related to the unknown airlight intensity A by the parameter P, which is the airlight degree of polarization. Without a polarizer the intensity is I^{total}. This intensity is comprised of the airlight intensity and the unknown direct transmission.

[2] In some kinds of high altitude clouds, anisotropic particles may have a macroscopic preferred directionality [9]. There, this statement may not hold, and a different analysis may be needed.

Figure 3. Images of the perpendicular and parallel polarization components. The parallel component has the best image contrast that optics alone can give, but in this case it is only slightly better than the contrast in the image of the worst polarization state. The raw images were acquired instantly, without waiting for changes in the visibility.

in Fig. 2, P relates the unknown airlight A to the difference between the intensity measurements, $I^\perp$ and $I^\parallel$.

We took images of a distant scene at different orientations of a polarizer. Fig. 3 shows the perpendicular and the parallel polarization components of the scene. The acquisition of the raw images was *not* conducted in the trivial situation described in Sec. 2.1.1: the haze was rather dense (visibility of a few kilometers), indicating the abundance of depolarizing multiple scatterings. For this reason, the parallel component has only a slight improvement of image contrast relative to the contrast in the perpendicular component. We note that due to the partial polarization of the airlight, $I^\parallel$ was darker than $I^\perp$. For clarity of display, the intensity of each of the photos shown in Fig. 3 is contrast-stretched, while the hue and saturation are as in the raw images. More details about obtaining these components are given in Appendix A.2.

4 Dehazing Images

For each image pixel, we have three unknowns: the object radiance (without haze) R, the airlight A and the scaled depth βz. These determine the intensity at each image pixel. The airlight is related to βz by Eq. (1). Thus, the number of unknowns per pixel is reduced to two. These unknowns can be estimated from *two* images taken at almost *any* general unknown (but non-degenerate) orientations of the polarizing filter. This is proved in Appendix A.1. However, the most stable results are obtained if the algorithm is based on $I^\parallel$ and $I^\perp$. Therefore, we focus on this case.

Let the raw images correspond to the estimated polarization components, $\hat{I}^\parallel$ and $\hat{I}^\perp$. Suppose we have an estimate of A_∞ and P. One way to estimate these global parameters is described in Sec. 7. From Eqs. (6-9), it can be seen that we can estimate the airlight of any point as

$$\hat{A} = \frac{\hat{I}^\perp - \hat{I}^\parallel}{P} \quad , \tag{11}$$

and the unpolarized image (Eq. 10) as

$$\hat{I}^{\text{total}} = \hat{I}^\parallel + \hat{I}^\perp \quad . \tag{12}$$

Using Eq. (5), the estimated direct transmission is therefore

$$\hat{T} = \hat{I}^{\text{total}} - \hat{A} \quad . \tag{13}$$

In this image the additive effect of the airlight is removed.

Recall that beside the addition of airlight, the haze attenuates the light coming from the object. The attenuation is estimated from Eqs. (1,11) as

$$\widehat{e^{-\beta z}} = 1 - \frac{\hat{A}}{A_\infty} \quad . \tag{14}$$

Thus, we can compensate for the attenuation of the transmitted light. From Eqs. (4,13,14) we obtain an estimate for the scene radiance that would have been measured in the absence of atmospheric scattering

$$\hat{R} = \frac{\hat{I}^{\text{total}} - \hat{A}}{\widehat{e^{-\beta z}}} = \frac{\hat{I}^{\text{total}} - \hat{A}}{1 - \hat{A}/A_\infty} \quad . \tag{15}$$

$\hat{R}$ is hence the dehazed image.

We note that A_∞, P and β are functions of the light wavelength λ. For instance [3, 8], in Rayleigh scattering $\beta \sim 1/\lambda^4$. For this reason the airlight in moderate haze is typically bluish. In order to account for the wavelength dependence, it is best to analyze the images with high spectral resolution. Since we only have RGB channels in our camera, we performed the analysis for each channel independently.

We applied these results to the images shown in Fig. 3. The resulting dehazed image[3] is shown in Fig. 4. The intensity of the displayed image has the same scale as was used when displaying[4] the "best polarized" image $I^\parallel$ on the bottom of Fig. 3. The contrast of features in the dehazed image is greatly improved relative to $I^\parallel$ and $I^\perp$. Moreover, the

[3] We did not apply the dehazing technique to the sky area. The reason is that the model assumes the sky to be at infinity, and thus there is no object to recover.

[4] As in the images shown in Fig. 3, only the intensity is scaled for the display, and the hue and saturation are not processed.

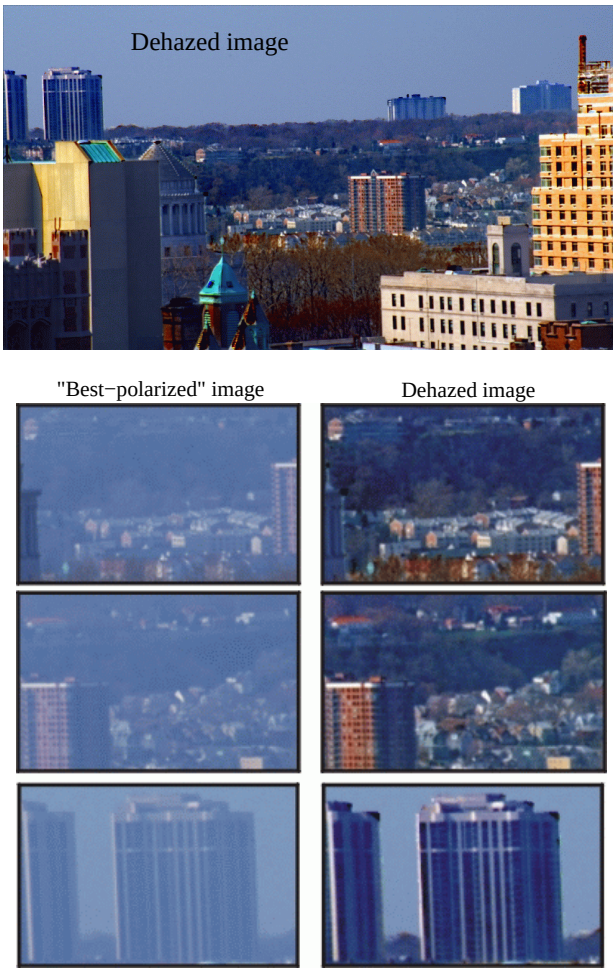

Figure 4. [Top] The dehazed image has much better contrast and color than what optical filtering alone yields, especially in the distant regions of the scene. [Bottom] In the magnified image portions, note the green forest and lawns, the red roofs of the distant houses and the clear white buildings on the ridge.

algorithm removed the blue color bias, which existed in the raw images. Thus the green forest is clearly visible in the distant scene, while in the raw images that area looks like grayish-blue noise. The colors of the red bricks and roofs of the distant buildings are also restored. The improvement of color is also seen in the closer objects, like the orange building on the right, where the blue airlight was weaker.

5 Range Map of the Scene

As a by-product of the dehazing process, we get an estimate of the range (depth) map of the scene. From Eq. (14)

$$\widehat{\beta z}(x,y) = -\log\left[1 - \hat{A}(x,y)/A_\infty\right] \quad . \tag{16}$$

Note that the estimated distance z is known up to a scale factor, which is the unknown scattering coefficient β.

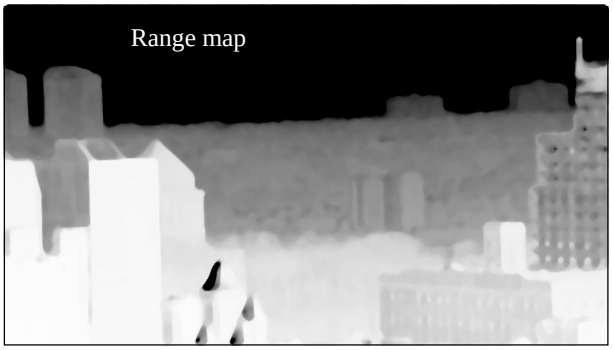

Figure 5. The range map of the scene, estimated as a by product of the dehazing algorithm. The farther the object, the darker the shade. Some surfaces of close objects are wrongly marked as distant ones due to their high degree of polarization.

Recall that we get an independent estimated range map for each color channel: $\widehat{\beta_\mathrm{r} z}$, $\widehat{\beta_\mathrm{g} z}$ and $\widehat{\beta_\mathrm{b} z}$, where the subscripts r, g, b denote the three color channels. These maps should be similar to each other, and only differ in their scale, which is set by the ratios of their scalar scattering coefficients, $\beta_\mathrm{r}, \beta_\mathrm{g}$, and β_b. We combine the range maps to a single, average one:

$$\overline{\beta z}(x,y) \equiv [\widehat{\beta_\mathrm{r} z}(x,y) + \widehat{\beta_\mathrm{g} z}(x,y) + \widehat{\beta_\mathrm{b} z}(x,y)]/3 \; . \tag{17}$$

We obtained a range map as a by-product[5] of dehazing the images shown in Fig. 3. It is shown in Fig. 5. In this figure, darker points correspond to more distant objects. The map is qualitatively consistent with the scene, indicating, for example, the close buildings, and the increase of distance uphill on the distant ridge. The range map also reveals the problems of the model. As discussed in Sec. 2.2, the degree of polarization of the distant, hazy objects is small relative to the airlight. For close objects, however, this may not be true. Indeed, a significant partial polarization was observed in some surfaces on the close buildings, especially those directly lit by the sun. In Fig. 5, this manifests in a "dark" shading of the points corresponding to these objects (rather than a "bright" shade). In those regions the algorithm suppresses the specularities.

6 Information about the Aerosols

In Sec. 4 we showed that based on as few as two images we can dehaze the imaged scene. Now we will show that based on the same raw images we can extract information about the atmospheric particles that degrade the scene visibility.

Consider the range maps of each color channel, that were described in Sec. 5. Averaging over the image pixels, we define scalars corresponding to each color channel

[5] To remove local outliers, we median filtered the map.

$$B_{\rm r} = \frac{\sum_{x,y} \widehat{\beta_{\rm r} z}(x,y)}{\sum_{x,y} \overline{\beta z}(x,y)} \quad , \tag{18}$$

$$B_{\rm g} = \frac{\sum_{x,y} \widehat{\beta_{\rm g} z}(x,y)}{\sum_{x,y} \overline{\beta z}(x,y)} \quad , \tag{19}$$

$$B_{\rm b} = \frac{\sum_{x,y} \widehat{\beta_{\rm b} z}(x,y)}{\sum_{x,y} \overline{\beta z}(x,y)} \quad . \tag{20}$$

These scalars express the scattering coefficients of the atmosphere, in each of the color channels, up to a single scale factor. This result is valuable because the relative scattering coefficients are determined by the size of the scattering particles [8, 9, 10]. Therefore, knowing these ratios supplies information about the distribution of the particles' size. This information can be incorporated in models that make explicit physical analysis of atmospheric scattering, as well as in applications of ecological monitoring. Using only RGB is a coarse sampling of the spectrum, and better information can be obtained with higher image spectral resolution. Nevertheless, the above analysis can be done with any spectral resolution.

In the experiment based on the images shown in Fig. 3, we obtained

$$\begin{bmatrix} B_{\rm r} \\ B_{\rm g} \\ B_{\rm b} \end{bmatrix} = \begin{bmatrix} 0.26 \\ 0.32 \\ 0.42 \end{bmatrix} \quad , \tag{21}$$

which means that the scattering in the blue band is about 60% stronger than the scattering in the red band. Had the dominant particles been small enough to obey Rayleigh's $1/\lambda^4$ rule, the scattering of the blue would have been more than 300% stronger than the red.

7 Estimating A_∞ and P

In order to dehaze the image we need an estimate of the global parameters A_∞ and P. Note that as $z \to \infty$

$$I^{\rm total} = Re^{-\beta z} + A_\infty (1 - e^{-\beta z}) \to A_\infty \quad . \tag{22}$$

The degree of polarization of the measured scene (i.e., the direct transmission combined with airlight) is

$$\hat{p}(x,y) = \frac{\hat{I}^{\perp}(x,y) - \hat{I}^{\parallel}(x,y)}{\hat{I}^{\perp}(x,y) + \hat{I}^{\parallel}(x,y)} \quad . \tag{23}$$

As $z \to \infty$,

$$\hat{p} \to \frac{A_\infty^{\perp} - A_\infty^{\parallel}}{A_\infty^{\perp} + A_\infty^{\parallel}} = P \, . \tag{24}$$

We can measure these parameters directly from the images. We can use points that are seen through enough haze (due to their distance) such that their radiance is practically not transmitted through it. Such points are not always available, so we use some heuristics to estimate these parameters.

The simplest way to estimate these parameters is to measure a patch of the sky at the horizon. Note that from Eqs. (11,12,13,23),

$$\hat{T}(x,y) = \frac{\hat{I}^{\rm total}(x,y)}{\hat{P}} \left[\hat{P} - \hat{p}(x,y) \right] \quad . \tag{25}$$

where $\hat{P}$ is the estimate of P. If our estimate of $\hat{P}$ is too low, then negative values can appear in the image of the direct transmission. This is especially relevant to distant objects, because $p(x,y) \to P$ when $z \to \infty$. Such errors can be expected when the sky patch measured is above the horizon. The reason is that haze density usually changes significantly as a function of altitude within the first few vertical kilometers of atmosphere [10], and even a few hundred meters.

In the experiment we performed, we first estimated $\hat{A}_\infty$ and $\hat{P}$ by measuring the sky values above the distant ridge across the images[6]. shown in Fig. 3. The average measured values of $\hat{P}$ were

$$\begin{bmatrix} \hat{P}_{\rm red} \\ \hat{P}_{\rm green} \\ \hat{P}_{\rm blue} \end{bmatrix} \approx \begin{bmatrix} 0.28 \\ 0.25 \\ 0.22 \end{bmatrix} \quad . \tag{26}$$

Indeed this heuristic method resulted in a slight error, and many of the resulting pixels of $\hat{T}$ and $\hat{R}$ had negative values, especially in the distant areas. We fine-tuned $\hat{P}$ by increasing its values globally by a few percent. This eliminated almost all the occurrences of negative values. This simple tuning is another heuristic we used. We are currently studying ways to automate the estimation of these parameters in a principled fashion, without relying on sky measurements.

Finally, note that $\hat{P}_{\rm red} > \hat{P}_{\rm green} > \hat{P}_{\rm blue}$. This is consistent with the literature [9, 20]: in haze, long wavelengths (red) are less depolarized (i.e., more polarized), compared to short (blue) wavelengths. As we noted before, the process of depolarization depends on the size and density of the scatterers [9]. Thus the estimation of P at the different spectral bands may provide additional information about the aerosols in the scene.

8 Discussion

We showed that image analysis that follows acquisition of polarization filtered images can remove the visual effects of haze. This approach enables dehazing when the problem cannot be solved by optics alone. In addition to the dehazed image, the method also yields information about scene structure and about the density and size distribution of the atmospheric particles. These results can form the basis for useful tools in photography and remote sensing.

Our method is based on the partial polarization of airlight. Therefore, its stability will decrease as the degree

[6] We allowed for a slight horizontal change of these parameters by fitting a 2^{nd} order polynomial to the measurements of $\hat{I}^{\perp}$ and $\hat{I}^{\parallel}$ of the sky above the ridge.

of polarization decreases. For instance, the method may be less effective under an overcast sky. The method may fail in situations of fog or very dense haze.

We are currently studying the effects of polarization in more complicated weather conditions such as fog or rain. Interestingly, the airlight in rain is partially polarized, and thus rainbows can be significantly enhanced or suppressed using a polarizer [9]. It is possible that this work can be extended to other scattering media. Examples for such media are underwater environments (where the ambient illumination is partially polarized [26]), or even tissues (e.g., skin).

Acknowledgments

This work was supported in parts by a grant from DARPA's Human Identification at a Distance program, award# N00014-00-1-0916, by the NSF award IIS-99-87979, and by the Morin Foundation.

A Appendix

A.1 Using Arbitrary 2 Images

In Sec. 4,5 we used estimates of $I^{\|}$ and $I^{\perp}$ in the dehazing algorithm. We now show that in theory the method can work based on two images taken at almost any different polarization orientations. Let $\theta_{\|}$ be the orientation of the polarizer for best transmission of the component parallel to the plane of incidence (Fig. 1). For a general orientation α, the observed airlight is

$$A(\alpha) = A\left\{1 - P\cos[2(\alpha - \theta_{\|})]\right\}/2 \ , \qquad (27)$$

which coincides with Eqs. (7,9) if $\alpha = \theta_{\|}, \theta_{\|} + 90^o$. Suppose we take two images of the scene with arbitrary orientations of the polarizer, $\alpha_1 \neq \alpha_2$. Because the direct transmission is unaffected by the polarizer orientation, the images are

$$I_1 = T/2 + A(\alpha_1) \qquad (28)$$

and

$$I_2 = T/2 + A(\alpha_2) \ . \qquad (29)$$

Let us define an effective airlight

$$A_{\text{effective}} \equiv A(\alpha_1) + A(\alpha_2), \qquad (30)$$

with an effective degree of polarization

$$P_{\text{effective}} \equiv \frac{A(\alpha_2) - A(\alpha_1)}{A_{\text{effective}}} \ , \qquad (31)$$

where we set $A(\alpha_2) \geq A(\alpha_1)$, without loss of generality. We also define an effective unfiltered image

$$I^{\text{total}}_{\text{effective}} \equiv I_1 + I_2 = T + A_{\text{effective}}. \qquad (32)$$

It can easily be shown that $A_{\text{effective}}$ is proportional to the actual airlight,

$$A_{\text{effective}} = fA = fA_{\infty}(1 - e^{-\beta z}) = A^{\text{effective}}_{\infty}(1 - e^{-\beta z}) \ , \qquad (33)$$

where $A^{\text{effective}}_{\infty}$ is the effective airlight at infinity (the horizon). The proportion factor f is

$$f = 1 - P\cos(\alpha_1 + \alpha_2 - 2\theta_{\|})\cos(\alpha_1 - \alpha_2) \ . \qquad (34)$$

Because we *do not know* $\theta_{\|}$ based on two arbitrary polarizer angles, f is unknown.

Suppose now that we have estimates of the parameters $P_{\text{effective}}$ and $A^{\text{effective}}_{\infty}$. These parameters can be estimated by measuring the sky intensities of I_1 and I_2, similar to the way described in Sec. 7. Then, we estimate the effective airlight at each point

$$\hat{A}_{\text{effective}} = \frac{I_2 - I_1}{P_{\text{effective}}} \ . \qquad (35)$$

From Eq. (32), the estimated direct transmission based on the raw images I_1 and I_2 is

$$\hat{T} = I^{\text{total}}_{\text{effective}} - \hat{A}_{\text{effective}} \ . \qquad (36)$$

From Eq. (33) the estimated attenuation is

$$\widehat{e^{-\beta z}} = 1 - \frac{\hat{A}_{\text{effective}}}{A^{\text{effective}}_{\infty}} \ , \qquad (37)$$

thus the dehazed image is

$$\hat{R} = \frac{I^{\text{total}}_{\text{effective}} - \hat{A}_{\text{effective}}}{1 - \hat{A}_{\text{effective}}/A^{\text{effective}}_{\infty}} \ . \qquad (38)$$

We can check the stability of using an arbitrary pair of images. It is easy to show that

$$P_{\text{effective}} = \frac{AP}{A_{\text{effective}}}\sin(\alpha_1 + \alpha_2 - 2\theta_{\|})\sin(\alpha_2 - \alpha_1) \ . \qquad (39)$$

Eq. (35) becomes unstable when $P_{\text{effective}} \to 0$. Beside the obvious case in which $P = 0$, this happens when

$$\frac{\alpha_1 + \alpha_2}{2} = \theta_{\|}, \theta_{\|} + 90^o \ . \qquad (40)$$

This is expected because the acquired images are equal if taken on symmetric angles relative to the extrema of the cosine in Eq. (27). Therefore, changing the orientation from α_1 to α_2 is degenerate. Except for these singular cases, dehazing is possible using two images. The best stability of dehazing is achieved when $P_{\text{effective}}$ is maximum, that is, when $\alpha = \theta_{\|}, \theta_{\|} + 90^o$. Therefore, our the paper focuses on dehazing based on $I^{\|}$ and $I^{\perp}$. The estimation of these images is discussed in the next section.

A.2 Using More than 2 Images

As mentioned above, the method works best with $I^{\|}$ and $I^{\perp}$. By rotating the polarizer to achieve an extremum of the intensity or contrast, it is often easy to visually detect the states corresponding to these components. However, it is easier and more accurate to estimate these components using *three* or more images taken through different general orientations of the polarizer. This is a common practice in polarization imaging [13, 19, 21, 22, 26].

Let $\theta_\parallel$ be the orientation of the polarizer for best transmission of the component parallel to the plane of incidence (see Figs. 1,2). For a general orientation α, the observed intensity at each pixel is

$$I(\alpha) = (1/2)I^{\rm total} - a\cos[2(\alpha - \theta_\parallel)] \qquad (41)$$

where a is the amplitude of the modulation caused by changing the filter's orientation.

We can write Eq. (41) for an angle α_k as

$$[1/2 \quad -\cos(2\alpha_k) \quad -\sin(2\alpha_k)] \begin{bmatrix} I^{\rm total} \\ a_{cos} \\ a_{sin} \end{bmatrix} = I_k \ , \qquad (42)$$

where $a_{cos} = a\cos(2\theta_\parallel)$ and $a_{sin} = a\sin(2\theta_\parallel)$. To obtain the estimates $\hat{I}^{\rm total}$, $\hat{a}_{cos}$ and $\hat{a}_{sin}$, three linearly independent measurements are sufficient. If we have more than 3 measurements, we derive the least squares estimates. Then, we find the image components as

$$\hat{I}^\parallel = (1/2)\hat{I}^{\rm total} - \hat{a} \qquad (43)$$

and

$$\hat{I}^\perp = (1/2)\hat{I}^{\rm total} + \hat{a} \ , \qquad (44)$$

where $\hat{a} = \sqrt{\hat{a}_{cos}^2 + \hat{a}_{sin}^2}$. These equations also yield an estimate of $\theta_\parallel$ at each pixel:

$$\hat{\theta}_\parallel = (1/2)\arctan(\hat{a}_{sin}/\hat{a}_{cos}) \ . \qquad (45)$$

The images shown in Fig. 3 were actually estimated this way, based on photographs taken at 4 different polarizer orientations. The photographs were linearized to compensate for the detector's radiometric response. The response was estimated from images of the Macbeth ColorChecker [5]. We obtained high dynamic range images by weighted averaging of multiple exposures.

References

[1] M. Ben-Ezra, "Segmentation with invisible keying signal," Proc. CVPR, pp. 32-37 (2000).

[2] C. F. Bohren, "Maximum degree of polarization of the resultant of two partially polarized incoherent beams," App. Opt. **26**, pp. 606-607 (1987).

[3] S. Chandrasekhar, *Radiative transfer*, pp. 24-37,280-284 (Dover, New York, 1960).

[4] F. Cozman and E. Krotkov, "Depth from scattering," Proc.CVPR, pp. 801-806 (1997).

[5] A. S. Glassner, *Principles of digital image synthesis*, Appendix G.4 (Morgan-Kaufmann, 1995).

[6] L. Grewe and R. R. Brooks, "Atmospheric attenuation reduction through multi-sensor fusion," Proc. SPIE **3376**, *Sensor fusion: Architectures, algorithms, and Applications II*, pp. 102-109 (1998).

[7] H. Farid and E. H. Adelson, "Separating reflections and lighting using independent components analysis," Proc. CVPR pp. 262-267 (1999).

[8] E. Hecht, *Optics*, 3^{rd} Ed., pp. 340-342 (Addison-Wesley, New-York, 1998).

[9] G. P. Können, *Polarized light in nature*, pp. 1-10,29-54,60-62,131-137,144-145 (Cambridge University Press, Cambridge, 1985).

[10] N. S. Kopeika, *A system engineering approach to imaging*, pp. 446-452 (SPIE Press, Bellingham 1998).

[11] S. G. Narasimhan and S. K. Nayar "Chromatic framework for vision in bad weather," Proc. CVPR, pp. 598-605 (2000).

[12] S. G. Narasimhan and S. K. Nayar "Removing weather effects from monochrome images," in these Proceedings of CVPR (2001).

[13] S. K. Nayar, X. S. Fang and T. Boult, "Separation of reflection components using color and polarization," Int. J. Comp. Vis. **21**, pp. 163-186 (1997).

[14] S. K. Nayar and S. G. Narasimhan, "Vision in bad weather," Proc. ICCV, pp. 820-827 (1999).

[15] J. P. Oakley, and B. L. Satherley "Improving image quality in poor visibility conditions using a physical model for contrast degradation," *IEEE Trans. Imag. Proc.* **7**, pp. 167-179 (1998).

[16] P. Pencipowski, "A low cost vehicle-mounted enhanced vision system comprised of a laser illuminator and range-gated camera," Proc. SPIE **2736** *Enhanced and synthetic vision*, pp. 222-227 (1996).

[17] M. Saito, Y. Sato, K. Ikeuchi, and H. Kashiwagi, "Measurement of surface orientations of transparent objects using polarization in highlight," Proc. CVPR, Vol. I, pp. 381-386 (1999).

[18] Y. Y. Schechner, J. Shamir and N. Kiryati "Polarization-based decorrelation of transparent layers: The inclination angle of an invisible surface," Proc. ICCV, pp. 814-819 (1999).

[19] Y. Y. Schechner, J. Shamir and N. Kiryati "Polarization and statistical analysis of scenes containing a semi-reflector," JOSA-A **17**, pp. 276-284 (2000).

[20] W. A. Shurcliff and S. S. Ballard, *Polarized light*, pp. 98-103 (Van Nostrand Co., Princeton, 1964).

[21] A. M. Shutov, "Videopolarimeters," Sov. J. Opt. Technol. **60**, pp. 295-301 (1993).

[22] J. E. Solomon, "Polarization imaging," App. Opt. **20**, pp. 1537-1544 (1981).

[23] B. T. Sweet and C. Tiana "Image processing and fusion for landing guidance," Proc. SPIE **2736** *Enhanced and synthetic vision*, pp. 84-95 (1996).

[24] K. Tan and J. P. Oakley, "Enhancement of color images in poor visibility conditions," Proc. ICIP pp. 788-791 (2000).

[25] L. B. Wolff, "Using polarization to separate reflection components," Proc. CVPR, pp. 363-369 (1989).

[26] L. B. Wolff, "Polarization vision: a new sensory approach to image understanding," Image and Vision Computing **15**, pp. 81-93 (1997).